Proceedings of ECOS 2021 - The 34th International Conference on
Efficiency, **C**ost, **O**ptimization, **S**imulation and **E**nvironmental Impact of Energy Systems
June 27-July 2, 2021, Taormina, Italy

Modelling of Energy Systems with Seasonal Storage and System State dependent Boundary Conditions using Time Series Aggregation and Segmentation

Alexander Holtwerth[a], André Xhonneux[b] and Dirk Müller[c,d]

[a] *Forschungszentrum Jülich, Institute of Energy and Climate Research, Energy Systems Engineering (IEK-10), Jülich, Germany, a.holtwerth@fz-juelich.de CA*

[b] *Forschungszentrum Jülich, Institute of Energy and Climate Research, Energy Systems Engineering (IEK-10), Jülich, Germany, a.xhonneux@fz-juelich.de*

[c] *RWTH Aachen University, E.ON Energy Research Center, Institute for Energy Efficient Buildings and Indoor Climate, Aachen, Germany, dmueller@eonerc.rwth-aachen.de*

[d] *Forschungszentrum Jülich, Institute of Energy and Climate Research, Energy Systems Engineering (IEK-10), Jülich, Germany, di.mueller@fz-juelich.de*

Abstract:
The optimization of planning is one of the challenging tasks for the optimal control of energy systems with seasonal storage. An optimization quickly becomes computationally intractable due to a high temporal resolution and a long time horizon needed for seasonal energy storage. Time series aggregation, in combination with additional time coupling constraints, can be used to reduce the size of the optimization problem drastically. However, some constraints of an energy system are directly dependent on the current system state and cannot be modeled as part of a typical period.
To preserve the computational advantages of time series aggregation with extra constraints for storage units while modeling a set of constraints with a full temporal resolution, we propose a method that uses a mapping between intra-period, inter-period, and full-resolution variables. Furthermore, we propose a separation of the year into different regions during the clustering. This leads to a decoupling of different regions of the year and therefore increases the flexibility of the optimization.
In a case study, we adopt the approach for an energy system with a dynamic hydrogen pipeline and a liquid organic hydrogen carrier (LOHC) storage system with a hot pressure swing reactor. By using full-resolution variables and a separation of the year in 3 different regions, we were able to reduce the computational time by 78% while maintaining an accuracy of 3% compared to an optimization with the full-time resolution.
The separation of the year into 3 regions lead to a consistent improvement in accuracy of up to 29.4% and a run time decrease of up to 82% compared to a clustering of the whole year in typical periods. Furthermore, a separation of the year into 3 regions extended the feasibility of the optimization problem to very low numbers of typical periods.

Keywords:
Renewable energy, Mixed integer linear programming, Time-series aggregation, Planning, Seasonal storage, Liquid organic hydrogen carrier (LOHC), Dynamic gas pipeline.

1. Introduction

Characteristics of renewable energies like photovoltaics (PV) or wind energy are high volatility on various time scales. Seasonal energy storage mitigates the effects of high volatility and increases the share of renewable energies used by the energy system [1]. Furthermore, an optimization of the planning for an energy system's operation increases the system's efficiency and accounts for the volatility of renewable energy sources. To optimize the planning of an energy system with seasonal storage, the consideration of a long time horizon is needed. However, modeling a long time horizon is a computationally challenging task since energy systems with renewable energy sources need to be modeled with a high time resolution [2]. Therefore, an optimization with a long time horizon quickly becomes intractable due to a high number of time steps and the accompanying increasing complexity of the optimization problem.
In recent studies, a significant focus is on developing methods to decrease the complexity of design optimizations for energy systems with seasonal storage [1, 3]. We can apply the same methods for the optimization of the planning to reduce the computational complexity. Therefore, we can derive more accurate models and find a better tradeoff between temporal resolution and model complexity.
Time series aggregation is widely used in literature for a reduction of the computational complexity of energy systems. A review on different time series aggregation methods can be found in [4]. Within the field of time series aggregation, the method of typical periods caught much attention over the past years. Kotzur et al. [3] adapted the method of typical periods to enable seasonal storage using inter-period variables. However, some system dynamics, like the pressure dependency of a component on a dynamic pipeline, depend on the current state of the system. Therefore, modeling these dynamics is not possible with inter-period variables since

the current pressure at any point in time is decisive for the operating behavior. In this paper, we extend the approach of Kotzur et al. [3] to cope with dynamics that depend on the system state using additional variables and constraints.
The case study in this paper considers a hybrid storage system with a battery and a hydrogen storage system since hydrogen enables seasonal storage of energy [5]. We consider a hydrogen storage system with a LOHC storage system to enable long-term hydrogen storage under ambient conditions [6] and a pressure storage tank to increase the system efficiency compared to a pure LOHC storage system.
The main contributions of this work are the following:

- Introduction of full-time resolution variables and constraints to the typical period approach
- Division of the year into different regions for time series aggregation
- The adaptation of time series aggregation to an energy system with state-dependent variables and constraints
- A parameter study of the influence of different time series aggregation methods on the accuracy and run time of an optimization of the planning

This work is structured as followed: In Section 2., we discuss the time series aggregation methods used in this work. The energy storage system and the component models are described in Section 3., followed by the computational results in Section 4.. Finally, Section 5. gives a summary and outlines the conclusion.

2. Time Series Aggregation Methods for Seasonal Storage

For a better understanding, we briefly explain the method of Kotzur et al. [3], our idea and motivation for a seperation of the year in different regions, and the usage of segmentation in section 2.1.. In section 2.2. we then describe the idea of coupling intra-period, inter-period, and full-time resolution variables.

2.1. Coupling of Typical Periods and Segmentation

In literature, typical periods are widely applied to optimizations with many time steps to reduce the system complexity. However, one of the major drawbacks is that the chronological order of time steps is only maintained within typical periods. To enable coupling of typical periods, Kotzur et al. [3] proposed a method that incorporates an additional set of variables between typical periods, namely the inter-period variables. For example, this method is used to couple the state of charge *soc* of typical periods to enable long-term energy storage. The difference between the *soc* at the beginning and the end of each typical period is used to calculate the value of each inter-period variable. Each period of the full-time series is represented by one typical period. Thus, we can define a mapping between typical periods and periods of the full-time series. An example for a mapping between *I* typical periods and *N* periods in the full-time series is shown in Table 1.

Table 1: Example of the relationship between periods in the full-time series (fts) and the representation by typical periods.

fts period	1	2	3	4	5	6	7	$\cdots$	N-2	N-1	N
typical period	1	2	1	1	3	2	1	$\cdots$	I	I-1	I

The coupling of typical periods can stiffen the optimization problem since a loading or unloading of the storage units needs to be possible at each point in time where the typical period appears. A typical period might appear in different situations regarding the system state and therefore lead to infeasibility for some operation strategies. For instance, some days in spring and autumn might be represented by the same typical period since the energy consumption and weather conditions are similar. However, the state of charge for seasonal storage is generally low in spring and high in autumn. Thus, a different operating strategy would be needed for optimal energy usage, but this is not possible if two periods in spring and autumn are represented by the same typical period.
To overcome this problem, we propose a division of the year into three different regions and derive typical days for each region separately. This does not change the formulation of the optimization problem as proposed by Kotzur et al. [3], but only changes the system input. A comparison between clustering the whole year in 60 typical days and clustering of three regions of the year into 20 typical days each is shown in Fig. 1.
The accuracy of the time series aggregation is decreased by dividing the year into different regions since some days that are similar cannot be represented by the same typical period. However, stiffening the optimization problem by typical periods that appear at different external conditions throughout the year can decrease the quality of an optimization problem even more.

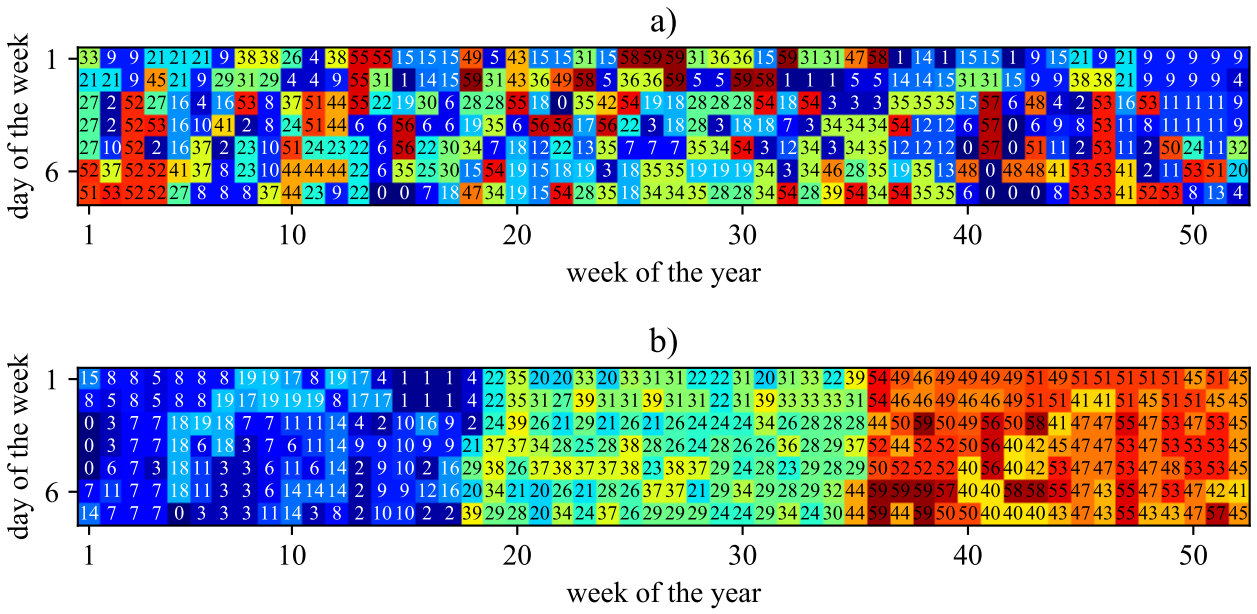

Figure 1: Distribution of typical days throughout the year as derived by clustering. In a) a clustering of the whole year in 60 typical days is visualized. b) shows a clustering of three regions with 20 typical days each.

Another addition to the coupling of typical periods is applied in this paper. Since start-up costs and energy losses are considered in many applications, we add an inter-period start-up variable st_n^{inter} to avoid free switching at the beginning of each typical period. Let $f_{\text{tp}}(n)$ be a function that maps the n-th period of the full-time series with $n \in \{1, 2, \cdots, N\}$, to the i-th typical period with $i \in \{1, 2, \cdots, I\}$, similar to the lookup Table 1. Furthermore, let $j \in \{1, 2, \cdots, J\}$ be the j-th time step of a typical period, then we can determine the value of the start-up variable by

$$st_n^{\text{inter}} \geq b^{\text{op}}{}_{f_{\text{tp}}(n),j=1} - b^{\text{op}}{}_{f_{\text{tp}}(n-1),j=J}, \tag{1}$$

$$st_n^{\text{inter}} \leq 1 - b^{\text{op}}{}_{f_{\text{tp}}(n-1),j=J}, \tag{2}$$

$$st_n^{\text{inter}} \leq b^{\text{op}}{}_{f_{\text{tp}}(n),j=1}. \tag{3}$$

Where $b^{op}{}_{f_{tp}(n),j=1}$ and $b_{op}{}_{f_{tp}(n),j=J}$ are the binary variables for the operational status of the first and the last segment of the i-th typical period that represents the n-th period in the full time series.
To further reduce the computational complexity, we use segmentation to reduce the number of time steps within one typical period. The idea of using segmentation in combination with typical periods was first introduced by Mavrotas et al. [8]. However, as stated by Hoffmann et al. [4], the trade-off between the resolution of intra-period variables and the number of periods has not been conclusively discussed. In this paper we use a combination of typical periods and segmentation since some constraints and variables are modeled in the full-time resolution. Thus, by reducing the full-time resolution, we can drastically reduce the system size while maintaining good model accuracy. The clustering in typical periods and segmentation is carried out using the open-source Python package tsam [9] with k-means clustering and agglomerative clustering, respectively.

2.2. Modeling of Intra-Period, Inter-Period, and Full-Time-Series Variables

The operating behavior of some systems depends on the current state of the system. Therefore, we model some constraints and variables in the full-time resolution to capture some essential system dynamics. The state of charge (*soc*) can be calculated using the superposition of inter-period variables and intra-period variables at any specific point in time. Let t be the j-th time step of the n-th period of the full-time resolution, and $f_{\text{inter}}(t)$ be a function that maps the t-th time step of the full-time resolution to the n-th inter-period variable. Furthermore, let $f_{\text{intra}}(t)$ be a function that maps the time step t of the full-time resolution to the j-th time step in the i-th typical period that represents the n-th period of the original time series. Then we can calculate the state of charge at time step t soc_t^{fts} by:

$$soc_t^{\text{fts}} = soc^{\text{inter}}_{f_{\text{inter}}(t)} + soc^{\text{intra}}_{f_{\text{intra}}(t)}. \tag{4}$$

Where soc^{inter} is an inter-period variable and soc^{intra} is an intra-period variable, respectively.

The relationship between intra-period, inter-period, and full-time series variables is shown in Fig. 2 for an exemplary state of chare *soc*. In Fig. 2 the *soc* of the 22-nd time step soc^{fts}_{22} is marked by a circle. In this example we can derive that $f_{\text{inter}}(t = 22) = 3$ and $f_{\text{intra}}(t = 22) = (1, 4)$ and calculate soc^{fts}_{22} using Eq. (4) by:

$$soc^{\text{fts}}_{t=22} = soc^{\text{inter}}_{n=3} + soc^{\text{intra}}_{i=1,j=4}. \tag{5}$$

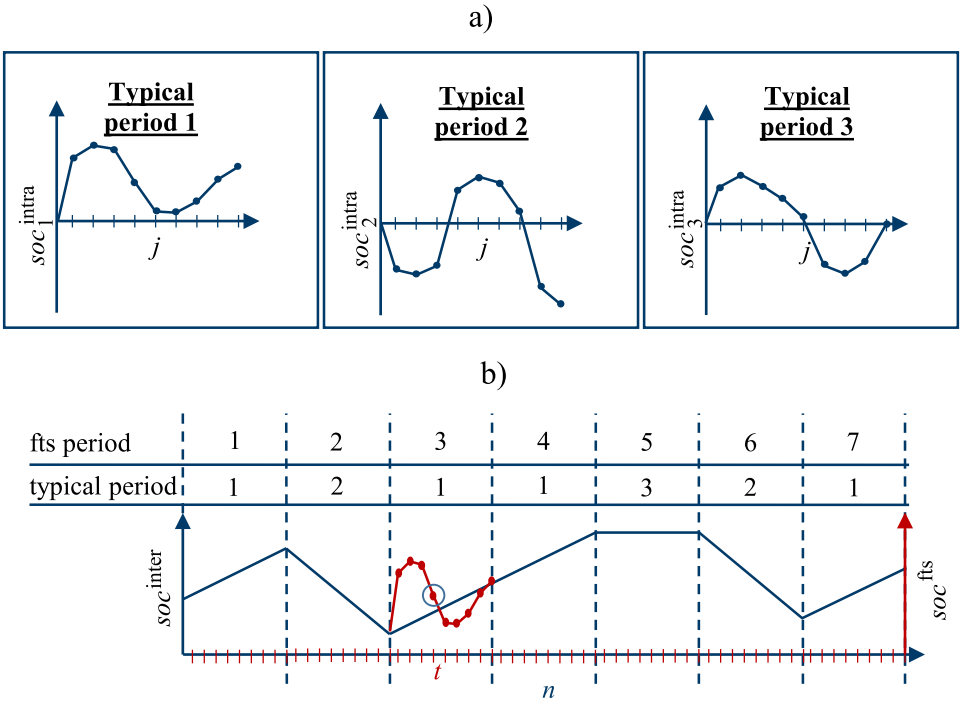

Figure 2: Example for the relationship between intra-period, inter-period, and full-resolution variables. In a) three different typical periods are shown, representing different periods of the full-time series as shown in b). In b) the 22-nd time step of the full-time series is circled. For this example, we can derive that $f_{\text{inter}}(t = 22) = 3$ and $f_{\text{intra}}(t = 22) = (1, 4)$.

We can use the mapping $f_{\text{intra}}(t)$ to further couple intra-period variables with full-time series variables. A variable v^{fts}_t of the time step t may be represented by a variable $v^{\text{intra}}_{f_{\text{intra}}(t)}$ to reduce the number of variables of an optimization problem. However, state-dependend variables need to be modeled in the full-time resolution, since intra period variables cannot account for different system states. Using all three variable types, namely the intra-period variables, inter-period variables, and full-resolution variables, we can construct equations that need to be modeled for each time step individually.
All variables and constraints in the full-time resolution increase the computational complexity. Therefore, it is essential to choose only the most important constraints for modeling in full-time resolution.

3. Case Study

The energy system considered in this case study is composed of an electrolyzer, a compressor, a fuel cell, a battery, a dynamic pipeline, a LOHC system, and a PV installation. The layout of the system is visualized in Fig. 3. The energy demand is derived from real-world measurements of office buildings with a time resolution of one year with hourly time intervals. A PV installation produces electricity that can be either directly used, stored in a battery, or converted into hydrogen using an electrolyzer. Additional electricity is directly bought from the grid at a variable grid price. The maximal grid usage is set to 20% of the yearly energy demand to increase the share of renewable energies.
The electrolyzer converts electrical energy to hydrogen that is then compressed to pipeline pressures. A large pressure tank is connected to the pipeline to increase the total volume of the pipeline and, therefore, its storage capacity. The LOHC is an additional storage capacity for the long-term storage of hydrogen. Finally, the fuel cell converts the hydrogen back to electricity. The whole system is modeled in the object-oriented modeling framework COMANDO [10].
The electrolyzer (ey) is modeled based on the model of Scheepers et al. [11] at a pressure of 5 bar for a Nafion 212 membrane. The fuel cell (fc) is modeled using the operating behavior described by Neisen et al. [12]. Since fuel cells and electrolyzers are highly modular [14], we can assume that the operating behavior of both technologies is scalable to the component size considered in this paper.

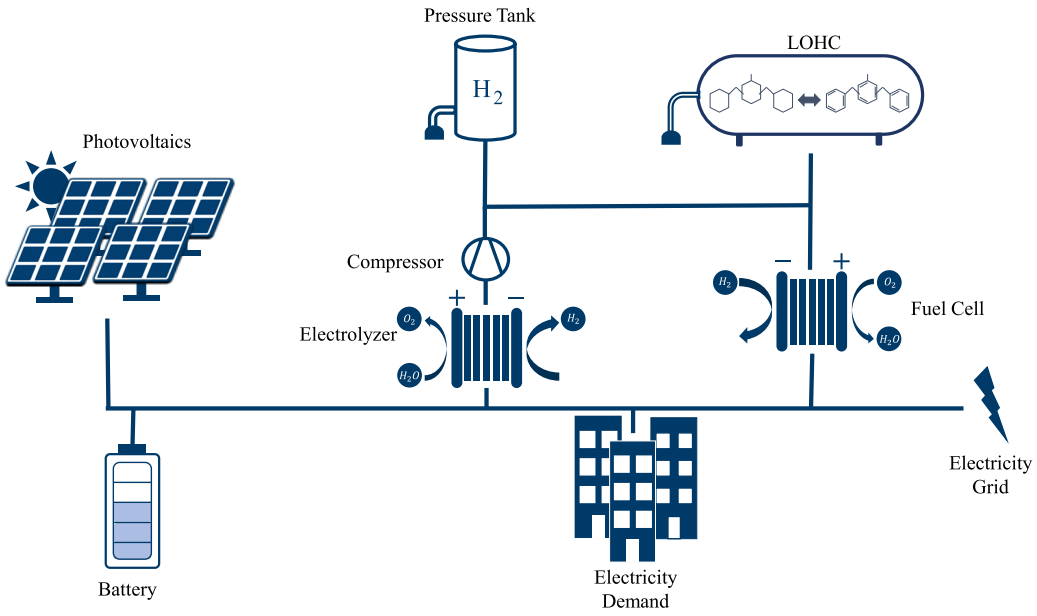

Figure 3: Sketch of the energy system.

The nonlinear operating behavior of the fuel cell and electrolyzer is modeled by equidistant sampling the operating behavior and then fitting a piecewise linear model with two linear elements to the generated data. We used the open-source Python package pwlf [13] to fit the piecewise linear function, and the multiple-choice MILP formulation as described by Vielma et al. [15]. Furthermore, the minimum power consumption and startup energy losses are modeled as describe by Neisen et al. [12] with additional coupling variables and constraints as described in 2.1.. All other variables and constraints of the electrolyzer and fuel cell are modeled as intra-period variables and constraints.

The LOHC system considered in this case study consists of a large storage tank and a hot pressure swing reactor. The hot pressure swing reactor is used for hydrogenation, and the dehydrogenation of the organic hydrogen carrier [16]. The dehydrogenation is carried out at a relatively low-pressure while a high pressure is needed for the hydrogenation [17]. Thus, we can only load the LOHC if the pipeline pressure $p_t^{\text{dp,fts}}$ is greater than the operating pressure of the LOHC $p^{\text{LOHC,op}}$. To model the pressure dependency we introduce one binary variable for the hydrogenation $b_{i,j}^{\text{LOHC,h}}$ and one for the dehydrogenation $b_{i,j}^{\text{LOHC,h}}$ as intra-period variables. Next, we define the constraint

$$b_{i,j}^{\text{LOHC,h}} \leq \frac{p_t^{\text{dp,fts}}}{p^{\text{LOHC,op}}}, \tag{6}$$

in the full-time resolution to set the binary variable $b_{i,j}^{\text{LOHC,h}}$ to 0 if the pipeline pressure is lower than the operating pressure of the LOHC reactor. Since $b_{i,j}^{\text{LOHC,h}}$ is defined as an intra-period variable, we lose accuracy because $p_t^{\text{dp,fts}}$ needs to be greater then $p^{\text{LOHC,op}}$ for all periods that are represented by one period in the typical period approach. However, due to the slow dynamics of the LOHC, we achieved good results using this simplification.

As a next step, we define equations for the minimal and maximal energy flow of the hydrogenation and dehydrogenation

$$w_{\text{min}}^{\text{LOHC,h}} \cdot b_{i,j}^{\text{LOHC,h}} \leq w_{i,j}^{\text{LOHC,h,intra}} \leq w_{\text{max}}^{\text{LOHC,h}} \cdot b_{i,j}^{\text{LOHC,h}}, \tag{7}$$

$$w_{\text{min}}^{\text{LOHC,dh}} \cdot b_{i,j}^{\text{LOHC,dh}} \leq w_{i,j}^{\text{LOHC,dh,intra}} \leq w_{\text{max}}^{\text{LOHC,dh}} \cdot b_{i,j}^{\text{LOHC,dh}}, \tag{8}$$

where $w_{\text{max}}^{\text{LOHC,h}}$, $w_{\text{max}}^{\text{LOHC,dh}}$, $w_{\text{min}}^{\text{LOHC,h}}$, and $w_{\text{min}}^{\text{LOHC,dh}}$ are the maximal and minimal energy flows of the hydrogenation and dehydrogenation, respectively. Equations 7 and 8 state that the energy flow $w_{i,j}^{\text{LOHC}}$ must be between the operation limits $w_{\text{min}}^{\text{LOHC}}$ and $w_{\text{max}}^{\text{LOHC}}$ for either the hydrogenation and dehydrogenation if the LOHC is in either operational state. In combination with Eq. 6, this means that the LOHC can only load if the pipeline pressure $p_t^{\text{dp,fts}}$ is greater than the operating pressure of the LOHC $p^{\text{LOHC,op}}$. The change of the state of charge $\Delta soc_{i,j}^{\text{LOHC}}$ is calculated by

$$\Delta soc_{i,j}^{\text{LOHC}} = \frac{w_{i,j}^{\text{LOHC,h,intra}} - w_{i,j}^{\text{LOHC,dh,intra}} / \eta^{\text{LOHC}} - st_{i,j}^{\text{LOHC,intra}} \cdot c^{\text{st,LOHC}}}{C^{\text{LOHC}}}, \tag{9}$$

where $st_{i,j}^{\text{LOHC,intra}}$ is a variable for the start-up of the LOHC, $c^{\text{st,LOHC}}$ is the start-up energy loss, η^{LOHC} is the dehydrogenation efficiency, and C^{LOHC} is the capacity of the LOHC. The exothermic hydrogenation releases heat

energy, while the dehydrogenation is an endothermic process. Since no waste heat utilization is considered in this work, we only consider the energy needed for the dehydrogenation in the form of a dehydrogenation efficiency η^{LOHC}. For simplicity, we consider electric heating of the LOHC reactor for the dehydrogenation and the resulting storage efficiency according to Müller et al. [7]. The start-up variable is modeled using intra-period constraints according to the equations by Neisen et al. [12]. As mentioned in 2.1. we add inter-period start-up variables according to Eq. (1) - (3) to avoid free switching between typical periods. Since $w_{\mathrm{min}}^{\mathrm{LOHC,h}} \geq c^{\mathrm{st,LOHC}}$, we can subtract energy loss of the inter-period start-ups from the state of charge of the LOHC

$$soc_n^{\mathrm{LOHC,inter}} = soc_{n-1}^{\mathrm{LOHC,inter}} + soc_{f_{\mathrm{tp}}(n),J}^{\mathrm{LOHC,intra}} - st_n^{\mathrm{LOHC,inter}} \cdot c^{\mathrm{st,LOHC}}. \tag{10}$$

Where $soc_{f_{\mathrm{tp}}(n),J}^{LOHC,intra}$ is the last time step of the i-th typical period that represents the n-th period of the full-time resolution, and $st_n^{\mathrm{LOHC,inter}}$ is the n-th inter-period start up variable.
The dynamic pipeline (dp) connects all hydrogen components and can be used as energy storage capacity due to its variable pressure. We use the ideal gas law to model the pipeline pressure since the compression factor for gaseous hydrogen is around one at pressures considered in this work.
The change of the state of charge of the pipeline $\Delta soc_{i,j}^{dp}$ is modeled as an intra-period variable:

$$\Delta soc_{i,j}^{\mathrm{dp}} = \frac{{w_{H2}}_{i,j}^{\mathrm{ey}} + {w_{H2}}_{i,j}^{\mathrm{LOHC,dh}} - {w_{H2}}_{i,j}^{\mathrm{LOHC,h}} - {w_{H2}}_{i,j}^{\mathrm{fc}}}{C^{\mathrm{dp}}}, \tag{11}$$

where the ${w_{\mathrm{H2}}}_{i,j}^{\mathrm{ey}}$ is the hydrogen output of the electrolyzer, ${w_{\mathrm{H2}}}_{i,j}^{\mathrm{fc}}$ is the hydrogen input of the fuel cell, and C^{dp} is the capacity of the pipeline. The state of charge is modeled according to the coupling of typical periods as explained by Kotzur et al. [3]. The pipeline pressure is, according to the ideal gas law, a linear function of the state of charge. Therefore, we define the pipeline pressure $p_t^{\mathrm{dp,fts}}$ as a function of the maximal and minimal pipeline pressure $p_{\mathrm{max}}^{\mathrm{dp}}$, $p_{\mathrm{min}}^{\mathrm{dp}}$ and the state of charge of the pipeline:

$$p_t^{\mathrm{dp,fts}} = \left(soc_{f_{\mathrm{inter}}(t)}^{\mathrm{dp,inter}} + soc_{f_{\mathrm{intra}}(t)}^{\mathrm{dp,intra}}\right) \cdot \left(p_{\mathrm{max}}^{\mathrm{dp}} - p_{\mathrm{min}}^{\mathrm{dp}}\right) + p_{\mathrm{min}}^{\mathrm{dp}}. \tag{12}$$

Note that effects of pressure losses over the length of the pipeline or a temperature dependency were not considered in this work.
The compressor model (comp) is derived using the equation for specific work of gas compression and a two-stage compressor as described by Tjarks [18]. Next, we use a data-driven modeling approach to generate a linear model. The compression factor $p_{\mathrm{out}}^{\mathrm{comp}}/p_{\mathrm{in}}^{\mathrm{comp}}$ for each compressor stage is assumed to be 3. The inlet pressure is set to 5 bar as the compressor is directly connected to the electrolyzer. Therefore, the operating behavior of the compressor is a bivariate function of the pipeline pressure $p_t^{\mathrm{dp,fts}}$ and the hydrogen output of the electrolyzer ${w_{H2}}_{i,j}^{\mathrm{ey}}$.
Next, we sample the two-dimensional operating range with equidistant points and then fit one linear element to the generated data points with a least-squares fit. One linear element does not capture the nonlinear dynamics of the operating behavior. However, since the compressor's electricity consumption is small compared to all other components, we do not need to model the operating behavior in detail to capture the most important system dynamics introduced by the compressor.
The electricity consumption ${w_{el}}_t^{\mathrm{comp,fts}}$ and the output pressure $p_t^{\mathrm{comp,fts}}$ of the compressor are modeled as variables in full-time resolution. The hydrogen input ${w_{H2}}^{\mathrm{comp,intra}}$ and the binary operating variable $b^{\mathrm{comp,intra}}$ are modeled as intra-period variables since the hydrogen input depends on the hydrogen output of the electrolyzer ${w_{H2}}^{\mathrm{ey,intra}}$

$${w_{H2}}_{i,j}^{\mathrm{comp,intra}} = {w_{H2}}_{i,j}^{\mathrm{ey,intra}} \tag{13}$$

and therefore, additional variables in the full-time resolution are unnecessary. We then model the electricity consumption in the full-time series as

$${w_{el}}_t^{\mathrm{comp,fts}} = c^{comp} \cdot b_{f_{\mathrm{intra}}(t)}^{\mathrm{comp,intra}} + b^{\mathrm{comp}} \cdot p_t^{\mathrm{comp,fts}} + a^{\mathrm{comp}} \cdot {w_{H2}}_{f_{\mathrm{intra}}(t)}^{\mathrm{comp,intra}}. \tag{14}$$

Where a^{comp}, b^{comp}, and c^{comp} are linear parameters determined by least-squares fitting. Furthermore, we add a minimal and maximal operating pressure and volume flow to the operating behavior

$$p_{\mathrm{min}}^{\mathrm{comp}} \cdot b_{f_{\mathrm{intra}}(t)}^{\mathrm{comp,intra}} \leq p_t^{\mathrm{comp,fts}} \leq p_{\mathrm{max}}^{\mathrm{comp}} \cdot b_{f_{\mathrm{intra}}(f)}^{\mathrm{comp,intra}}, \tag{15}$$

$${w_{H2}}_{\mathrm{min}}^{\mathrm{comp}} \cdot b_{i,j}^{\mathrm{comp,intra}} \leq {w_{H2}}_{i,j}^{\mathrm{comp,intra}} \leq {w_{H2}}_{\mathrm{max}}^{\mathrm{comp}} \cdot b_{i,j}^{\mathrm{comp,intra}}. \tag{16}$$

Where $p_{\mathrm{min}}^{\mathrm{comp}}$ and $p_{\mathrm{max}}^{\mathrm{comp}}$ are the maximal and minimal operating pressure, and ${w_{H2}}_{\mathrm{min}}^{\mathrm{comp}}$ and ${w_{H2}}_{\mathrm{max}}^{\mathrm{comp}}$ are the minimal and maximal hydrogen flows through the compressor.

The battery (bat) is modeled with a constant charge and discharge efficiency similar to the battery model by Gabrielli et al. [1]. Therefore, we can derive the change of the state of charge of the battery $\Delta soc_{i,j}^{\text{bat}}$ by

$$\Delta soc_{i,j}^{\text{bat}} = \frac{w_{c_{i,j}}^{\text{bat,intra}} \cdot \eta^{\text{bat,c}} - w_{dc_{i,j}}^{\text{bat,intra}} / \eta^{\text{bat,dc}}}{C^{\text{bat}}}. \tag{17}$$

where $w_{c_{i,j}}^{\text{bat,intra}}$ and $w_{dc_{i,j}}^{\text{bat,intra}}$ are the charging and discharging energy flows, $\eta^{\text{bat,c}}$ and $\eta^{\text{bat,dc}}$ are the charging and discharging efficiencies, and C^{bat} is the battery capacity. Next, we introduce a binary variable $b_{i,j}^{\text{bat,intra.}}$ to avoid charging and discharging at the same time and limit the charging and discharging energy flow:

$$w_{c_{i,j}}^{\text{bat,intra}} \leq b_{i,j}^{\text{bat,intra}} \cdot w_{c_{\text{max}}}^{\text{bat}}, \tag{18}$$

$$w_{dc_{i,j}}^{\text{bat,intra}} \leq \left(1 - b_{i,j}^{\text{bat,intra}}\right) \cdot w_{dc_{\text{max}}}^{\text{bat}}. \tag{19}$$

In these equations, $w_{c_{i,j}}^{\text{bat,intra}}$ and $w_{dc_{i,j}}^{\text{bat,intra}}$ are the maximal charging and discharging energy flows of the battery. The state of charge is modeled using inter-period variables as described by Kotzur et al. [3].
We define the the objective function as the operational cost of energy system

$$Obj = \sum_{t=1}^{T} w_{el_t}^{\text{grid,buy}} \cdot c_t^{\text{grid}} \cdot \Delta t_t \tag{20}$$

where $w_{el_t}^{\text{grid,buy}}$ is the electricity purchased from the grid at a grid price c_t^{grid} at the t-th timestep with the time step length Δt_t. We choose the operational cost of the energy system as the objective function since we do not consider a design optimization and no other operational goals like reducing CO_2 emissions. The grid price c_t^{grid} is the trading price of 2019 in Germany [19]. The sizing of the components is listed in table 2.

Table 2: Assumed component sizes.

Component property	$w_{H2_{\text{max}}}^{\text{ey}}$	$w_{H2_{\text{max}}}^{\text{fc}}$	C^{bat}	C^{LOHC}	C^{dp}
Value	1166 kW	932 kW	4.118 MWh	811.23 MWh	62.72 MWh

4. Results

We optimize the operation of the energy system with a varying number of typical days, segments for each typical day, and regions per year to validate the method. Afterward, we compare the results to an optimization that we ran with the full-time series and no time series aggregation. The optimizations are carried out using Gurobi 9.0 [20] with a time limit at 4000s, a MIP Gap of 3% and a value for the share of heuristics at 20%.
To evaluate the results of the optimization, we examine the resulting optimal state of charge for each storage technology. For a first visual comparison, we compare the results of the optimization with the full-time series, with the results of an optimization with 10 typical days and an optimization with 60 typical days, with 12 segments and 3 yearly regions each. The state of charge of the battery is highly volatile and cannot be predicted accurately by an optimization with a low number of typical days, as shown in Fig 4.
Fig. 5 shows the state of charge of the dynamic pipeline and the LOHC. The resulting state of charge of the dynamic pipeline and the LOHC for an optimization with 60 typical days are very similar to the results of the optimization with the full-time series. Furthermore, the optimization with 10 typical days is able to capture a similar behavior of the state of charge throughout the year but with lower accuracy. However, the results show that the modeling of some constraints in full-time resolution enables optimization with state-dependent system dynamics. The optimizations with 10 and 60 typical days were both able to capture the dynamic of a reduced state of charge during the first months of the year. Furthermore, both optimizations were able to determine the ideal point in time to increase the pipeline pressure to enable hydrogenation of the liquid organic hydrogen carrier.
To further validate the results, we define some measures to quantify the quality of the optimization results. One measure is the difference of the objective value determined by the optimizations:

$$\Delta Obj = \frac{Obj_{tsa} - Obj_{fts}}{Obj_{fts}} \tag{21}$$

Where Obj_{fts} is the objective value of the optimization with the full-time series, and Obj_{tsa} is the objective value of an optimization with time series aggregation. The resulting ΔObj for different optimizations conducted in the present case study are shown in Fig. 6.

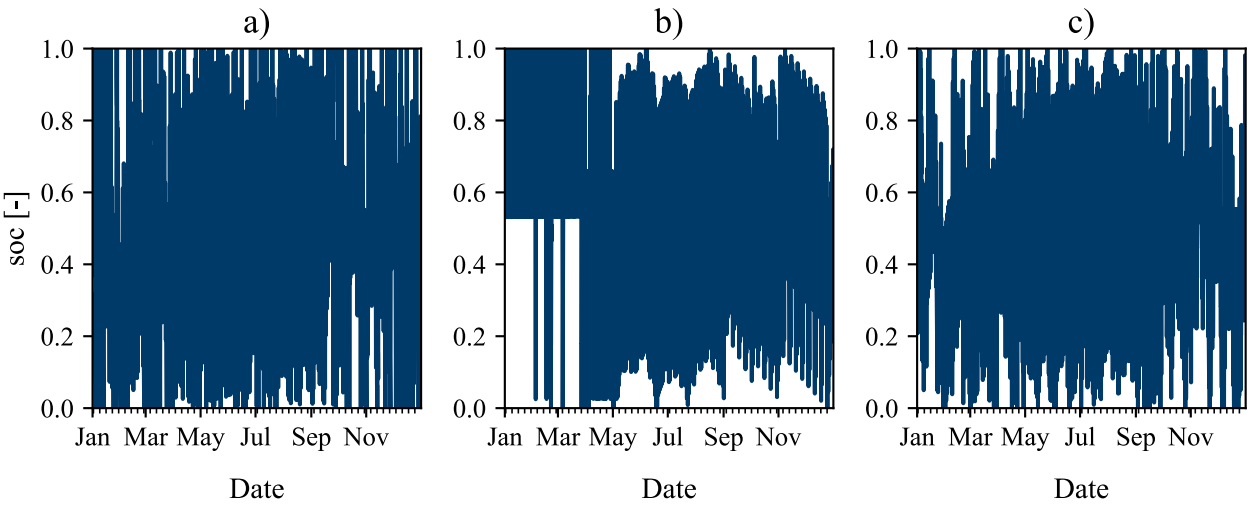

Figure 4: The predicted optimal state of charge of the battery throughout the year for a) the full-time series, b) 10 typical days divided into 3 regions with 12 segments each day, and c) 60 typical days divided into 3 regions with 12 segments each day.

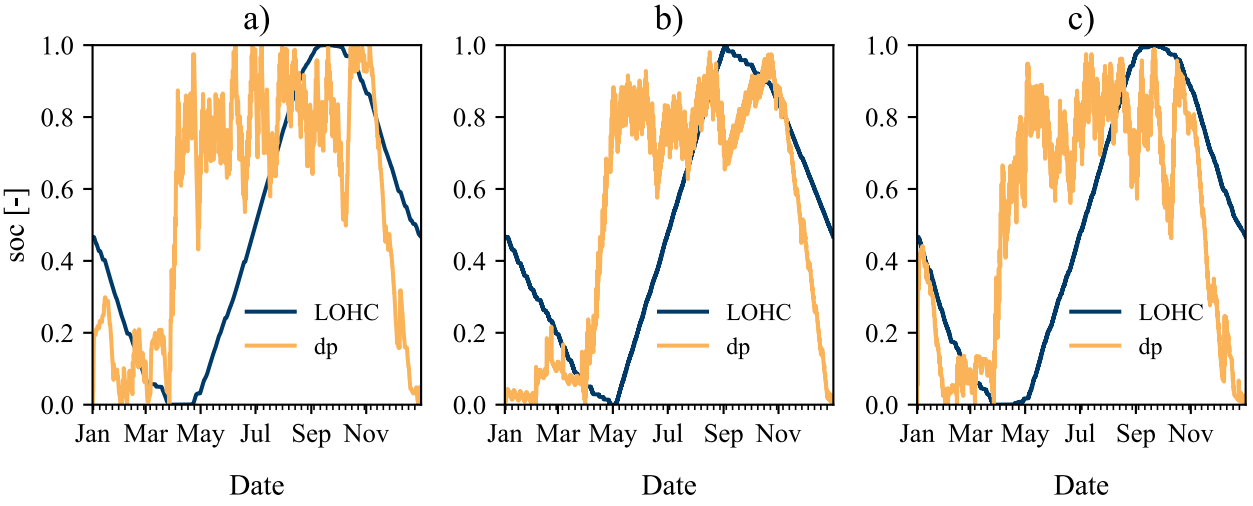

Figure 5: The predicted optimal state of charge of the LOHC, and dynamic pipeline (dp) throughout the year for a) the full-time series, b) 10 typical days divided into 3 regions with 12 segments each day, and c) 60 typical days divided into 3 regions with 12 segments each day.

As shown in Fig. 6, the ΔObj generally decreases with an increasing number of typical days. The ΔObj increases for 120 typical days and 24 segments because the optimization reaches the time limit with a significant remaining optimality gap. Some optimizations, like the optimization with 24 segments and 60 typical days with one region per year, do not produce an upper bound within the optimization timelimit. Optimizations that did not produce an upper bound are not included in Fig. 6.
Figure 7 shows the run time of the different optimizations. We do not show optimizations that do not produce an upper bound within the time limit in Fig. 7 since we consider the optimization to be failed as no usable operational strategy can be derived from the results.
Furthermore, we include a measure for the difference of the state of charge for the different storage technologies:

$$\Delta SOC = \frac{\sum_t |soc_t^{tsa} - soc_t^{fts}|}{\sum_t soc_t^{fts}}. \tag{22}$$

Equation (22) describes the deviation of the predicted state of charge for each storage technology from the optimal state of charge at each time step t. soc_t^{tsa} is the state of charge of a storage technology at time step t calculated using time series aggregation, and soc_t^{fts} is the state of charge of a storage technology at time step t calculated using the full-time series. The results of the parameter study are shown in Table 3.

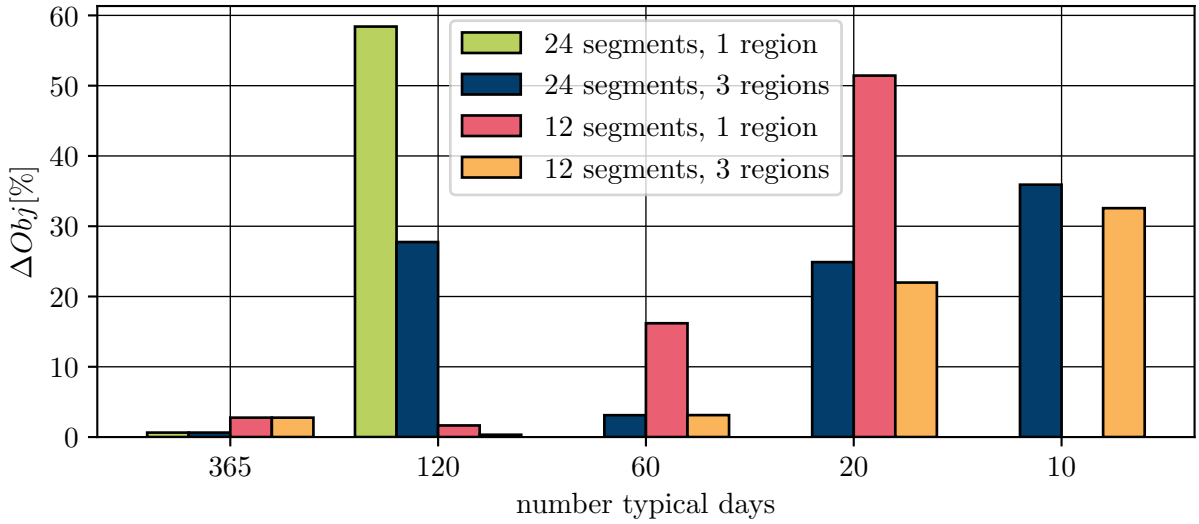

Figure 6: ΔObj for operational optimizations with 10, 20, 60, 120, and 365 typical days per year, with a separation of the year in one and three regions, and segmentation in 24 and 12 segments per day.

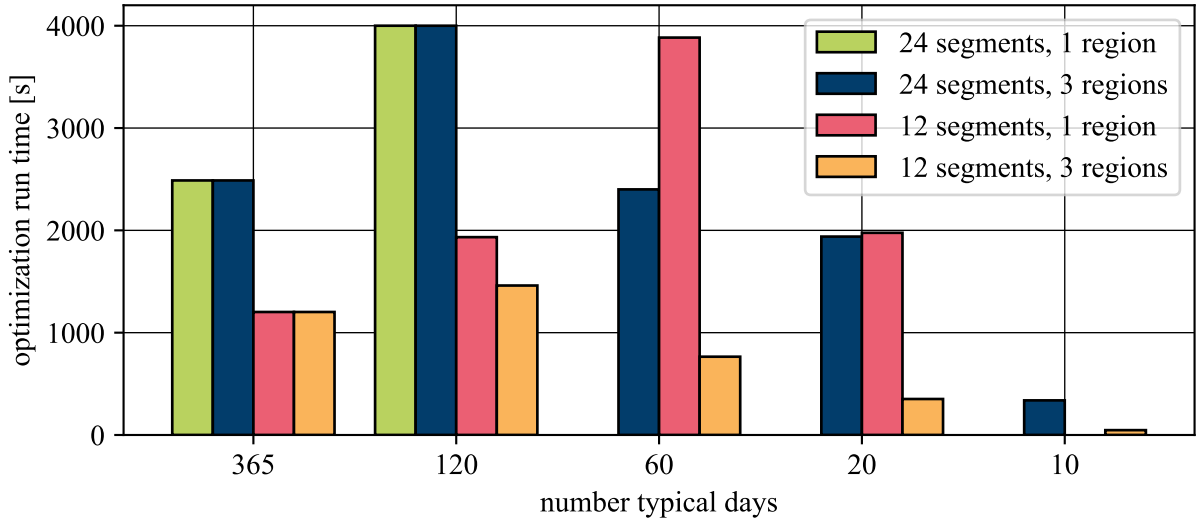

Figure 7: Optimization run times for operational optimizations with 10, 20, 60, 120, and 365 typical days per year, with a separation of the year in one and three regions, and segmentation in 24 and 12 segments per day.

The first number of the settings in the first column of Table 3 is the number of typical days used for the optimization, the second is the number of segments for each day, and the third number is the number of regions for each year. As shown in the last row of the Table, the results with 365 typical days and 24 hours per typical day are almost exactly the same as the original solution. The slight differences can be explained by the 3% MIP Gap and the resulting possibility for different near-optimal solutions.
The influence of the number of typical days on the run time and accuracy of the optimization can be seen by comparing the results of optimizations with 10, 20, 60, and 120 typical days, 12 segments per day, and 3 regions per year. The run time increases as expected with an increasing number of typical days. However, the optimization with 120 typical days yields no computational advantage compared to 365 typical days in this case study. Therefore, we do not investigate higher numbers of typical days.
A very low number of typical days leads to a high deviation from the full-time series optimization. Comparing the different values for the ΔSOC of the different storage technologies, we can see that the state of charge of the LOHC and the pipeline are reasonably well estimated, but the calculated state of charge of the battery deviates from the full-time series. This is due to the high volatility of the state of charge of the battery.
Next, we evaluate the influence of the division of the year in different regions for clustering. As shown in Table 3, an optimization with a small number of typical days might become infeasible if we do not divide

Table 3: Comparison between different settings for the optimization of the planning of the energy system. The optimization with the full-time series *fts* is listed as a reference for the optimization time. The first number of the settings is the number of typical days used for the optimization, the second is the number of segments for each day, and the third number is the number of regions for each year.

Settings	t_{opt}	ΔObj%	ΔSOC battery	ΔSOC dp	ΔSOC LOHC
fts	3543	0	0	0	0
10/12/1	infeasible	-	-	-	-
10/12/3	47	32.5	0.404	0.185	0.076
10/24/1	infeasible	-	-	-	-
10/24/3	338	35.9	0.406	0.191	0.090
20/12/1	1976	51.4	0.394	0.270	0.090
20/12/3	351	22.0	0.362	0.182	0.038
20/24/1	4000	-	-	-	-
20/24/3	1939	24.9	0.355	0.178	0.058
60/12/1	3884	16.2	0.337	0.243	0.065
60/12/3	765	3.1	0.312	0.139	0.028
60/24/1	4000	-	-	-	-
60/24/3	2400	3.1	0.285	0.124	0.033
120/12/1	1933	1.6	0.320	0.117	0.021
120/12/3	1460	0.3	0.290	0.123	0.030
120/24/1	4000	51.4	0.264	0.122	0.64
120/24/3	4000	27.7	0.257	0.110	0.041
365/12/1	1202	0.3	0.184	0.060	0.007
365/24/1	2487	0.6	0.097	0.050	0.016

the year into different regions. Furthermore, in this case study, we were able to increase the accuracy and reduce the optimization's run time by dividing the year into 3 different regions. However, the high number of coupling constraints between typical days might cause this extreme dependency on the division of the year in regions. Further studies are needed to conclusively determine whether this holds true for the original formulation proposed by Kotzur et al. [3].
Finally, we evaluate the influence of the segmentation on the run time of the optimization. As shown in Table 3, segmentation decreases the runtime drastically. The percentage computation time savings are particularly high for a small number of typical days. This might be due to the reduction of full-time series variables and constraints since segmentation reduces the number of time steps per year, and hence the reduction of variables and constraints due to clustering in typical days becomes more important.

5. Conclusion

In this paper, we were able to show that we can model system state-dependent variables and constraints with an extra set of variables in full-time resolution and an appropriate mapping between intra-period, inter-period, and full-time resolution variables. Furthermore, we were able to show that in some cases, we can increase the accuracy and reduce the run time of an optimization by separating the year in different regions for the clustering in typical periods. In the case study presented in this paper we were able to increase the accuracy by up to 29% and decrease the run time of the optimization by up to 82% by dividing the year in 3 regions prior to the clustering without changing the formulation of the optimization problem. This shows that in future works, a focus on data preparation can lead to additional computational advantages compared to a sheer focus on the formulation of the optimization problem.
In the case study presented in this paper, the best trade-off between accuracy and run time was achieved by dividing the year into 3 regions and clustering each region with 20 typical days, to a total number of 60 typical days, with 12 segments each. A reduction of 78% of the run time was achieved while maintaining an accuracy of 3% compared to an optimization with the full-time resolution. Furthermore, if only a rough estimation of the state of charge of the hydrogen storage system is needed, a much lower number of typical periods can be used.

Acknowledgments

The authors would like to thank their colleagues for fruitful discussions. Part of this work was funded by the German Federal Ministry of Education and Research within the research project "LLEC::P2G++ / Saisonale Speicherung in gekoppelten, regenerativen Energiesystemen mittels Power-to-Gas (P2G): Demonstration großskaliger Wasserstoffspeicherung mittels innovativer LOHC-Technologie im Verbund mit einer KWK-Anlage, dynamis-

cher Pipeline und Rückverstromung durch AFC-Brennstoffzelle" (03SF0573). The support is gratefully acknowledged.

References

[1] Gabrielli P., Gazzani M., Martelli E., and Mazzotti M. *Optimal design of multi-energy systems with seasonal storage*, Applied Energy, 2018; 219:408–424

[2] Poncelet, K., Delarue, E., Duerinck, J., Six, D., and D'haeseleer, W. *The importance of integrating the variability of renewables in long-term energy planning models*, Report, KU Leuven,, 2014; Available from `https://www.mech.kuleuven.be/en/tme/research/energy_environment/Pdf/wp-importance.pdf`

[3] Kotzur L., Markewitz P., Robinius M., and Stolten D. *Time series aggregation for energy system design: Modeling seasonal storage.*, Applied Energy, 2018; 213:123–135

[4] Hoffmann M., Kotzur L., Stolten D., and Robinius M. *A review on time series aggregation methods for energy system models.*, Energies, 2020; 13(3):641

[5] Reuß M., Grube T., Robinius M., Preuster P., Wasserscheid P., and Stolten D. *Seasonal storage and alternative carriers: A flexible hydrogen supply chain model*, Applied Energy, 2017; 200:290-302

[6] Müller K., Stark K., Emel'yanenko V. N., Varfolomeev M. A., Zaitsau D. H., Shoifet E., Schick C., Verevkin S. P., and Arlt W. *Liquid organic hydrogen carriers: thermophysical and thermochemical studies of benzyl-and dibenzyl-toluene derivatives*, Industrial & Engineering Chemistry Research, 2015; 54(32), 7967-7976

[7] Müller K, Thiele S., and Wasserscheid P. *Evaluations of concepts for the integration of fuel cells in liquid organic hydrogen carrier systems*, Energy & Fuels,, 2019; 33(10):10324–10330

[8] Mavrotas G., Diakoulaki D., Florios K., and Georgiou P. *A mathematical programming framework for energy planning in services' sector buildings under uncertainty in load demand: The case of a hospital in athens.*, Energy Policy, 2008; 36(7):2415–2429

[9] Kotzur L, Hoffmann M., Markewitz P., Robinius M, and Stolten D. *tsam—time series aggregation module.*, 2017, Available at: `https://github.com/FZJ-IEK3-VSA/tsam`, [accessed 30.01.2021]

[10] Langiu M., Shu D. Y., Baader F. J., Hering D., Bau U., Xhonneux A., Müller D., Bardow A., Mitsos A., and Dahmen M. *COMANDO: A Next-Generation Open-Source Framework for EnergySystems Optimization*, 2021, arXiv preprint arXiv:2102.02057

[11] Scheepers F., Stähler M., Stähler A., Rauls E., Müller M., Marcelo C. and Lehnert W. *Improving the efficiency of pem electrolyzers through membranespecific pressure optimization.*, Energies, 2020; 13(3):612

[12] Neisen V., Baader F. J., and Abel D. *Supervisory model-based control using mixed integer optimization for stationary hybrid fuel cell systems*, IFAC-PapersOnLine, 2018; 51(32), 320-325

[13] Jekel C. F. and Venter G. *pwlf: A python library for fitting 1d continuous piecewise linear functions*, 2019; Available from `https://github.com/cjekel/piecewise_linear_fit_py` [accessed 30.01.2021]

[14] Gabrielli P., Gazzani M., and Mazzotti M. *Modeling fuel cells in integrated multi-energy systems*, Energy Procedia, 2017; 142:1407–1413

[15] Vielma J. P., Ahmed S., and Nemhauser G. *Mixed-integer models for nonseparable piecewise-linear optimization: Unifying framework and extensions.*, Operations Research, 2010; 58(2):303–315

[16] Jorschick H., Preuster P., Dürr S., Seidel A., Müller K., Bösmann A., and Wasserscheid P. *Hydrogen storage using a hot pressure swing reactor*, Energy & Environmental Science, 2017; 10(7):1652–1659

[17] Jorschick H., Dürr S., Preuster P., Bösmann A., and Wasserscheid P. *Operational stability of a lohc-based hot pressure swing reactor for hydrogen storage.*, Energy Technology, 2019; 7(1):146–152

[18] Tjarks G. *PEM-Elektrolyse-Systeme zur Anwendung in Power-to-Gas Anlagen [dissertation]*, Rheinisch-Westfälische Technische Hochschule Aachen. Aachen; 2017; Available from: `https://publications.rwth-aachen.de/record/689617`

[19] Bundesnetzagentur | SMARD.de, 2021, Available from: `https://www.smard.de/home/marktdaten`

[20] Gurobi Optimization LLC. *Gurobi Optimizer Reference Manual*, 2021; Available from: `http://www.gurobi.com`